Schmidt, A., C. W. Rella, M. Göckede, C. Hanson, Z. Yang, B. E. Law (2014). Removing traffic emissions from CO_2 time series measured at a tall tower using mobile measurements and transport modeling. Atmospheric Environment 97, 94-108.

Removing traffic emissions from CO_2 time series measured at a tall tower using mobile measurements and transport modeling

Andres Schmidt[1*], Chris W. Rella[2], Mathias, Göckede[3], Chad Hanson[1], Zhenlin Yang[1], Beverly E. Law[1]

[1] *Oregon State University,* Corvallis, Oregon, USA

[2] *Picarro Inc., Santa Clara, California, USA*

[3] *Max Planck Institute for Biogeochemistry, Jena, Germany*

Abstract

In recent years, measurements of atmospheric carbon dioxide with high precision and accuracy have become increasingly important for climate change research, in particular to inform terrestrial biosphere models. Anthropogenic carbon dioxide emissions from fossil fuel burning have long been recognized to contribute a significant portion of the carbon dioxide in the atmosphere. Here, we present an approach to remove the traffic related carbon dioxide emissions from mole fractions measured at a tall tower by using the corresponding carbon monoxide measurements in combination with footprint analyses and transport modeling. This technique improves the suitability of the CO_2 data to be used in inverse modeling approaches of atmosphere-biosphere exchange that do not account for non-biotic portions of CO_2. In our study region in Oregon, road traffic emissions are the biggest source of anthropogenic carbon dioxide and carbon monoxide. A three-day mobile campaign covering 1700 km of roads in northwestern Oregon was performed during summer of 2012 using a laser-based Cavity Ring-Down Spectrometer. The mobile measurements incorporated different roads including main highways, urban streets, and back-roads, largely within the typical footprint of a tall CO_2 observation tower in Oregon's Willamette Valley. For the first time, traffic related CO:CO_2 emission ratios were measured directly at the sources during an on-road campaign under a variety of different driving conditions. An average emission ratio of 7.43 (±1.80) ppb CO per ppm CO_2 was obtained for the study region and applied to separate the traffic related portion of CO_2 from the mole fraction time series. The road traffic related portion of the CO_2 mole fractions measured at the tower site reached maximum values ranging from 9.8 to 12 ppm, depending on the height above the surface, during summer 2012.

1 Introduction

Atmospheric carbon dioxide measurements with high precision and accuracy have become a vital part of research on the sources and sinks of CO_2 from the local to global scale. Anthropogenic emissions of CO_2, in particular combustion products, are an ever increasing component of atmospheric CO_2 (e.g. IPCC, 2013; Friedlingstein et al., 2010; Bergeron and Strachan, 2011; Peters et al., 2012), creating unique challenges for quantifying terrestrial uptake and release of CO_2 across regions. The challenges are especially acute in regions where both anthropogenic and biogenic sources have significant influence on the atmospheric measurements. Thus, the use of "natural" CO_2 ratios that do not include anthropogenic contributions is critical to be able to adjust carbon cycle models to better capture the real variability in carbon cycle processes. Using atmospheric CO_2 mixing ratio data to inform inverse carbon flux models requires separation of the biotic from anthropogenic components. Large errors and biases in the biospheric model can be introduced by attributing anthropogenically induced spatio-temporal changes in atmospheric CO_2 to photosynthesis and respiration processes, and vice versa. Typically, anthropogenic emissions within the footprint of a given tower are removed by subtracting the emission inventory for these gases, so that what is left is the effect of the biosphere. However, the efficacy of this method is limited by the quality of the inventory, which can be highly inaccurate, especially on hourly and daily time scales, as well as on the kilometer level spatial scales.

Several data products are available for providing larger scale background CO_2 levels or even to assess the CO_2 portions attributed to various anthropogenic sources (e.g. Peters et al., 2007; Gurney at al., 2009). These products usually provide spatial resolutions that are not suitable for high resolution regional or local scale analyses and/or are not available in a sub-daily temporal resolution. Moreover, since these products are based on a sparse network of measurement sites to represent large inhomogeneous areas (Wang et al., 2013) or on remote sensing data (Oda and Maksyutov, 2011), they often exhibit biases in regions where the density of measurements is low or no measurements are available at all to constrain modelled or interpolated values in those regions (e.g. Göckede et al., 2010, Pillai et al., 2011).

Although the quality improved over recent years, gridded datasets that provide information about CO_2 emissions still suffer from insufficient data sources and are often associated with large relative uncertainties of 60% or more (Wang et al., 2013).

Carbon monoxide can be used to separate anthropogenic CO_2 from biotic sources (Vogel et al., 2010; Turnbull et al., 2011; LaFranchi et al., 2013), provided the emission ratios of the two gases is known.

Atmospheric CO mainly originates from incomplete combustion processes such as vehicle emissions, oil or gas burning, or biomass burning. In addition, atmospheric CO occurs as a byproduct of the oxidation of hydrocarbons (Granier et al., 2000). CO has a relative short lifetime of only several weeks in the troposphere as opposed to CO_2 because it is either oxidized to CO_2 in a photochemical reaction with oxygen or in a direct reaction with the radical OH at ambient temperatures (Finlayson-Pitts and Pitts, 2000; Brasseur et al., 2003).

In regions with urban areas and dense road traffic infrastructure the CO emissions are mostly defined by the abundance and strength of anthropogenic sources such as road traffic and heating (e.g. Fogg and Sangster, 2003; Seinfeld and Pandis, 2006) which makes CO a useful tracer for various gases also originating from anthropogenic emissions including CO_2 (Chen et al., 2013) and in particular to correlate the CO:CO_2 emissions from traffic (Wang et al., 2010; Lavaux et al., 2013, Popa et al., 2014).

Automobile exhaust is the major source of CO in the Unites States. In urban areas, motor vehicles account for up to 95% of the CO emissions (US-EPA, 2003). With a contribution of 86% of the CO emissions in Oregon, traffic combustions from on-road vehicles are the dominant source of CO in our study region (US-EPA, 2013). Other sources of CO in Oregon are other fuel combustion processes (9.3%), industrial processes (2.2%), and miscellaneous other sources (2.4%).

In addition, the total transportation related direct combustion emissions sector accounts for 34% of Oregon's total CO_2 emissions (ODT, 2009) which makes traffic also the largest source of anthropogenic CO_2 in Oregon.

Using the traffic emission ratios measured directly on the roads allows us to account for this varying portion of traffic related CO_2 sampled at a tall tower in the Willamette Valley.

Here we present a signal decomposition method to remove the transit portion from CO_2 measured at a tall tower by applying the CO:CO_2 emission ratio for the vehicle fleet found in the study area. By removing the CO_2 portion that is associated with on-road traffic the suitability of the CO_2 mole fractions for inverse biosphere-atmosphere carbon cycle modeling can be increased.

2 Data and Measurements

2.1 Tower measurements and instrumentation for high-precision CO and CO_2 mole fractions

In this study we are using the data from three measurement towers in Oregon. Equipped with Cavity Ring-Down Spectrometers (CRDS G2032, Picarro, Inc., Santa Clara, CA), the measurement towers provide high accuracy measurements of CO and CO_2 mixing-ratios and water vapor. In addition, the towers are equipped with instrumentation for standard meteorological measurements (wind speed and direction, air temperature, and humidity).

The Silverton tower is located in the Willamette Valley about 7 km east of the town of Silverton (44.9986° N, 122.6948° W, elevation: 351 m a.s.l.). It is the tallest tower of the Oregon network with its highest sample inlet at 269 m above ground level. Due to the exposed location on top of a smoothly graded hill overlooking the Willamette Valley this tower monitors integrated signals from the entire NW sector of Oregon. Most of Oregon's population resides in 3 metropolitan areas in the Willamette Valley urban corridor. The tower inlets sample air that is influenced by urban emissions from the densely populated Salem area (~18 km to the West) and fossil fuel emissions from the Portland metropolitan area about 40 km to the north during respective wind conditions. In addition, the interstate highway I-5 goes through the entire valley in a distance of 22 km west of the Silverton tower with an annual average daily traffic (AADT) of 50,000 – 100,000 vehicles / day (ODT, 2011).

Measurements at the Silverton tower started in July 2012. The core of the tower instrumentation is a CRDS analyzer G2302 for CO_2/CO/H_2O that sequentially measures a vertical profile consisting of 4 inlets at 31, 51, 121, and 269 m above ground level.

The Walton tower is located in the center of the Oregon Coast Range, about 44 km West of Eugene, OR and about 4 km northeast of the small town of Walton, OR (44.0664° N, 123.6292° W, elevation: 715 m a.s.l.).

Observations at the Walton site started in February 2012. The tower has a height of 80 m and is located on a hilltop, with no significant sources of anthropogenic emissions in the near field footprint. The mole fraction time series captured at the Walton tower show significant effects of CO_2 release and uptake by the surrounding Douglas-fir forest, and are intended to provide information on the effect of climate variability on the very productive mesic forest ecosystems along the West Coast. The tower is equipped with a CRDS analyzer measuring CO_2/CO/H_2O with a 0.4 Hz sampling rate, rotating through a vertical profile of 3 inlet heights at 30, 50, and 72 m above ground.

The Mary's Peak tower is located only 49 km to the north of the Walton tower and is also located in the Oregon Coast Range Mountains. Therefore both towers represent similar environmental conditions and are located within the same ecosystem mostly covered by Douglas fir (*Pseudotsuga menziesii*) forest.

In contrast to the Walton tower the Mary's Peak tower frequently captures the incoming air from the Pacific Ocean with background concentrations of trace gases during conditions with continuous westerly wind directions and stable atmospheric stratification during nighttime or during inversions when the tower is situated well above the boundary-layer. The CO and CO_2 mole fractions in this air masses are unaffected by concentration changes due to regional anthropogenic emissions or uptake/release by vegetation and soil. This is mainly attributed to its exposed position as the highest point of the Oregon Coast Range (44.5043° N, 123.5525° W, elevation: 1250 m a.s.l.), 45 km from the Pacific. The measurement height is 10 m above ground above an open meadow on the mountain top.

2.2 The CO_2 / CO Cavity Ring-Down Spectrometer:

For both the mobile and tower-based measurements, we used CO/CO_2/H_2O analyzers based on cavity ring down spectroscopy (CRDS) (Model G2302, Picarro, Santa Clara, CA, USA), an optical technology in which direct measurement of infrared absorption loss in a sample cell is used to quantify the mole fraction of the gas. Two separate lasers are used in the analyzers described here.

Light from each laser, tuned to specific near-infrared absorption features of the key analyte molecules, is directed sequentially into an optical resonator (called the optical cavity). The optical cavity consists of a closed chamber with three highly reflective mirrors, and it serves as a compact flow cell with a volume of less than 10 standard cm^3 into which the sample gas is introduced. The flow cell has an effective optical path length of 15-20 km; this long path length allows for measurements with high precision (with ppb or even parts-per-trillion uncertainty, depending on the analyte gas), using compact and highly reliable near-infrared laser sources.

The gas temperature and pressure are tightly controlled in these instruments (Crosson, 2008). This stability allows the instrument (when properly calibrated to traceable reference standards) to deliver accurate measurements that need very infrequent calibration relative to other CO_2 and CO instrumentation. The instrument employs active control of the optical wavelength, which delivers sub-picometer wavelength targeting on a microsecond timescale. Ringdown events are collected at a rate of about 200 ringdowns per second. Individual spectrograms consist of about 50 to 300 individual ringdowns (or 0.25 - 1.5 seconds), distributed across 10-20 spectral points around the peak. The overall measurement interval is about 2.5 seconds. The resulting spectrograms are analyzed using nonlinear spectral pattern recognition routines, and the outputs of these routines are converted into gas concentrations using linear conversion factors derived from calibration using standards that are traceable to the WMO scales for CO_2 and CO.

The spectroscopy of CO_2 and CO is nearly identical to the algorithms that in another standard model (the G2401) from the same manufacturer, with the notable exception that the water vapor line used in the G2302 (at 6280.42 wavenumbers) is different from the line used in the G2401 that is used to report water vapor and to calculate the dry-mole fraction of CO_2, which is located at 6057.80 wavenumbers. Even in the G2401, the line at 6280.42 wavenumbers is used to calculate the dry mole fraction of CO, so that the results in Chen et al. 2013 apply to the instruments used in this study. From dry-mole fraction measurements of CO performed in the laboratory on these instruments, we find that the total uncertainty in the dry-mole fraction of CO due to errors in the water vapor correction to be 5 ppb (k = 2, 95% coverage factor).

The dry-mole fraction of CO_2 has been studied extensively using the water vapor line at 6057.80 wavenumbers. Therefore, for these studies to be applicable to the G2302, it is necessary to perform a cross-comparison of the two water vapor measurements.

The cross-comparison was performed on an instrument that reports both water vapor lines (model G2401, S/N CFKADS-2009, Picarro, Inc, Santa Clara, CA, USA) over a range of water from 0 - 6 % (in H_{rep}). From this experiment, the following calibration between the two water lines is obtained:

$$H_{rep} = a'H_{G2302} + b'H_{G2302}^2 \quad (1)$$

Here, H_{rep} is the reported spectroscopic measurement of water vapor (in %) for the G2401 that has not been corrected for self-broadening. The coefficients in this equation are *a'* = 0.91925 and *b'*= 0.020223. Using the self-broadening correction in Winderlich et al. (2010), we find the following expression for water vapor concentration, which has been corrected for the nonlinearity caused by self-broadening of the water vapor line and tied to the NIST-traceable hygrometer used in Winderlich et al. (2010):

$$H_{act} = AH_{G2302} + BH_{G2302}^2 + CH_{G2302}^3 \ , \quad (2)$$

where A = 0.70966, B = 0.032084, and C = 0.000724.

In addition, using the above relation, we have determined the dry-mole fraction correction of CO_2 to be given by the following cubic equation:

$$\frac{CO_{2wet}}{CO_{2dry}} = 1 - aH_{G2302} - bH_{2302}^2 - cH_{G2302}^3 \ , \quad (3)$$

in which a = -0.01103, b = -0.0004686 and c = -9.94 x 10^{-6}. These coefficients are based entirely on the cross-calibration experiment described above and the standard coefficients first described in Chen et al. (2010) and validated in Rella et al. (2013). We therefore take advantage of the uncertainties described in Rella et al. (2013), which states that the water correction achieves an uncertainty of 0.1 ppm (1σ) up to 2.5% water vapor content (H_{rep}). This limit safely covers all data used in this study.

2.3 Quality assurance and uncertainty of the tower gas measurements

To account for instrument drift we apply a calibration cycle every 50 hours. For CO_2 we use standard gases produced in our lab that are traceable to the WMO X2007 scale (Tans et al., 2009) with an expanded calibration uncertainty of ≤ 0.15 ppm (k=2).

This expanded uncertainty incorporates the component uncertainties of the WMO primary scale, the ESP-1000 transfer calibration, the individual secondary standard calibration, and a coverage factor (k) applied to set the confidence interval of the uncertainty to the 95% level. In practice, our calibration system was assessed in the 2011 WMO 5th blind round robin and found to agree with the WMOX2007 scale within ≤ 0.03ppm for CO_2 (NOAA, 2012).

The sampling schedule for all systems used within this study has been set up to go through all profile levels at the respective site, while also facilitating regular calibration sequences. For the multi-inlet systems, air is drawn continuously through ½ inch Synflex tubing (Eaton Corp., Sumter, SC, USA) from all inlet heights separately using a separate oil-free piston pump (617 CA32, Gardner Denver Thomas GmbH, Puchheim, Germany) for each inlet. 10 µm filters (1R416, Solberg Manufacturing Inc., Itasca, IL, USA) at all inlets protect the system from coarse particles.

In addition, a 1 µm PTFE filter (ACRO® 50, Pall Corp., Port Washington, NY, USA) is mounted just in front of the analyzer sample inlet.

Flow meters (AWM5104VN, Honeywell, Fort Washington, PA, USA) are used to assure a continuous flow of ambient air with a flow rate of 10 lpm. To prevent compromised data due potential leaks the flow meters are placed behind the gas subsample inlets (Fig. 1).

A subsampling system consisting of a sample manifold with up to 8 ports (4 calibration gases + number of inlets) is attached to the main lines. The solenoid valves (TM10 series, Numatics Inc., Novi, MI, USA) are controlled by a CR1000 data logger (Campbell Scientific Inc., Logan, Utah, USA) valve sequencer software to direct a chosen sample from a distinct inlet height or calibration tank into the Picarro CRDS analyzer (Figure 1). The outlet of the G2302 is connected to a diaphragm pump (MZ 2C NT, Vacuubrand GmbH & CO KG, Wertheim, Germany) to maintain the pressure of 140 torr in the measurement cell of the CRDS.

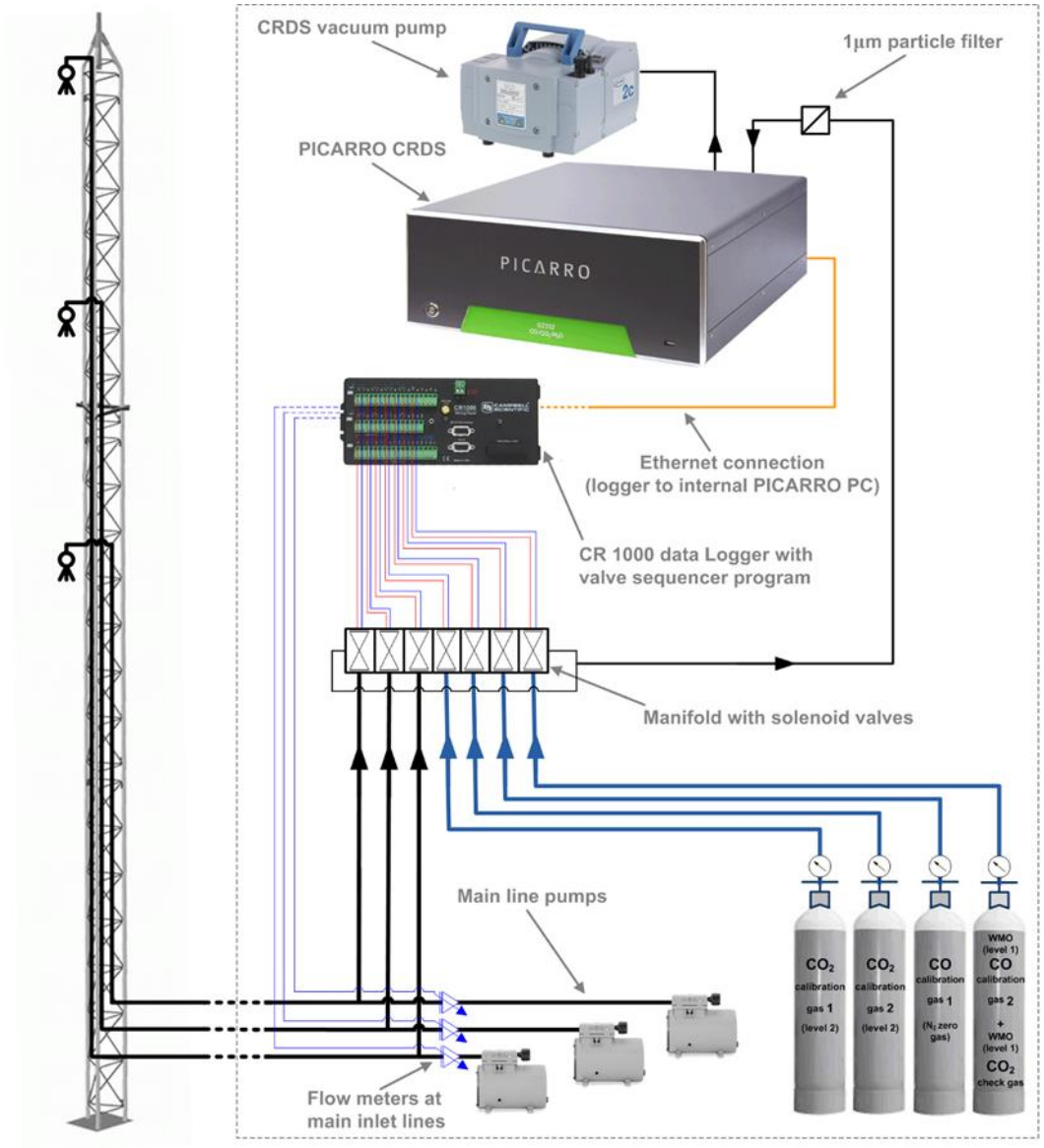

Figure 1: Schematic of measurement system setup at the CO/CO_2 observation towers in Oregon.

Every 50 hours we run a sequence of 4 calibration gases (2 for CO_2 and 2 for CO) consecutively through the G2302, for 7.5 minutes each. For each calibration cycle, a first order polynomial fit using known target mole fractions from the calibration tanks and the mean mole fractions from the corresponding measurements is calculated. The final coefficients for the linear regression are calculated from a linear interpolation between the two adjacent calibrations and then applied to the data between those two calibration cycles.

The set of calibration gases at each rower consist of two level 2 gas tanks for CO_2 and one level 1 gas tank in combination with an ultrapure N_2 zero gas (99.9999% purity) for CO (Fig. 1).

The WMO standard used for the calibration of the CO measurements also provides an additional, well defined CO_2 value that is not used for the actual CO_2 correction. This additional value is used to assess the uncertainty of the corrected final CO_2 mole fractions. During the analyzed period from July 1 2012 through September 30 2012, the average difference between the known WMO standard and the corresponding, corrected CO_2 values during the calibration intervals was 0.136 ppm (number of calibration intervals = 79) with a standard deviation of 0.011 ppm. This value confirms that in practice the measurements are well within the expanded uncertainty which incorporates the uncertainties of the level 2 CO_2 calibration gases produced in the OSU lab and the uncertainty of the measurement device itself (±0.15 ppm).
In addition, the deviation between the primary WMO standard in the NOAA lab and the tank deployed at the Silverton CO/CO_2 system during the calibration in the NOAA lab needs to be considered for error propagation calculations. The total uncertainty is then given by:

$$\delta_{CO_2} = (\delta^2{}_{meas} + \delta^2{}_{ref} + \delta^2{}_{lab/site} + \delta^2{}_{H_2O})^{1/2}. \qquad (4)$$

Where δ_{ref} is the uncertainty of the WMO working standards used as a final reference which is documented as ±0.071 ppm (Zhao and Tans, 2006). $\delta_{lab/site}$ is the average standard deviation between the NOAA WMO level 1 standard and the WMO level 1 standard tank for the Silverton site during the three CO_2 tank calibration at NOAA and is 0.01 ppm (σ=0). δ_{meas} gives the average deviation between the WMO standard and the measurements that are corrected based on level 2 calibration gases. δ_{H_2O} represents the uncertainty added by the water vapor correction of the CRDS (Rella et al., 2013). Thus, after error propagation considering all single incorporated uncertainties the overall uncertainty of the CO_2 mole fraction values is ±0.184 ppm for the interval analyzed in this study.

However, unlike for the CO_2 corrections there was no additional reference value for CO available that was not incorporated in the linear correction. Hence, the given uncertainty is the cumulative uncertainty after error propagation according to Eq. 4 including:

a.) the standard deviation during the 50-hour calibration intervals using the CO span calibration gas at the site (1.236 ppb),

b.) the 2% working standard uncertainty of the NOAA CO standard (WMO 2010),

c.) the average standard deviation of the two calibrations for the tank at NOAA that is reported to be 0.185 ppb (σ=0.007), and

d.) the water vapor correction error for CO given as 5 ppb ($\pm 2\sigma$).

Thus, applying the 2% estimate to the absolute value of our WMO level 1 CO calibration gas (272.5 ppb), the total uncertainty for the CO mole fractions used within this study is of ±7.50 ppb.

2.4 Mobile on-road measurements of CO_2 and CO

In July 2012, a 3-day field survey was conducted in the Willamette Valley of Oregon. An automobile was equipped with a real-time $CO/CO_2/H_2O$ analyzer (G2302, S/N CKADS-2035) and a GPS with sub-meter resolution (R100, Hemisphere GPS, Scottsdale, AZ, USA). The instrumentation was powered directly from the automobile electrical system, using an inverter to convert the 12V DC source to 120V AC suitable for powering the CRDS. The inlet tube supplying the instrument was affixed to the roof of the vehicle. Over three days, the instrument was driven over 1,700 km throughout the Northwest portion of Oregon. The measurements were concentrated in the Willamette Valley on main highways, back roads along forests, agricultural areas, and Oregon's largest urban centers. Moreover, some sections were also driven in the Coast Range, along the Pacific coast, downtown areas of Portland and Eugene, the Columbia Plateau east of Portland on Interstate 84, as well as within the Cascade Mountains east of the Willamette Valley. Maximum mole fractions of 2310 ppb CO and 566 ppm CO_2 were measured during the mobile road campaign.

The urban areas and the main roads and Interstate routes are located within the main footprint area of the Silverton tower and therefore affect the measurements of the CO and CO_2 mole fractions (Fig. 2).

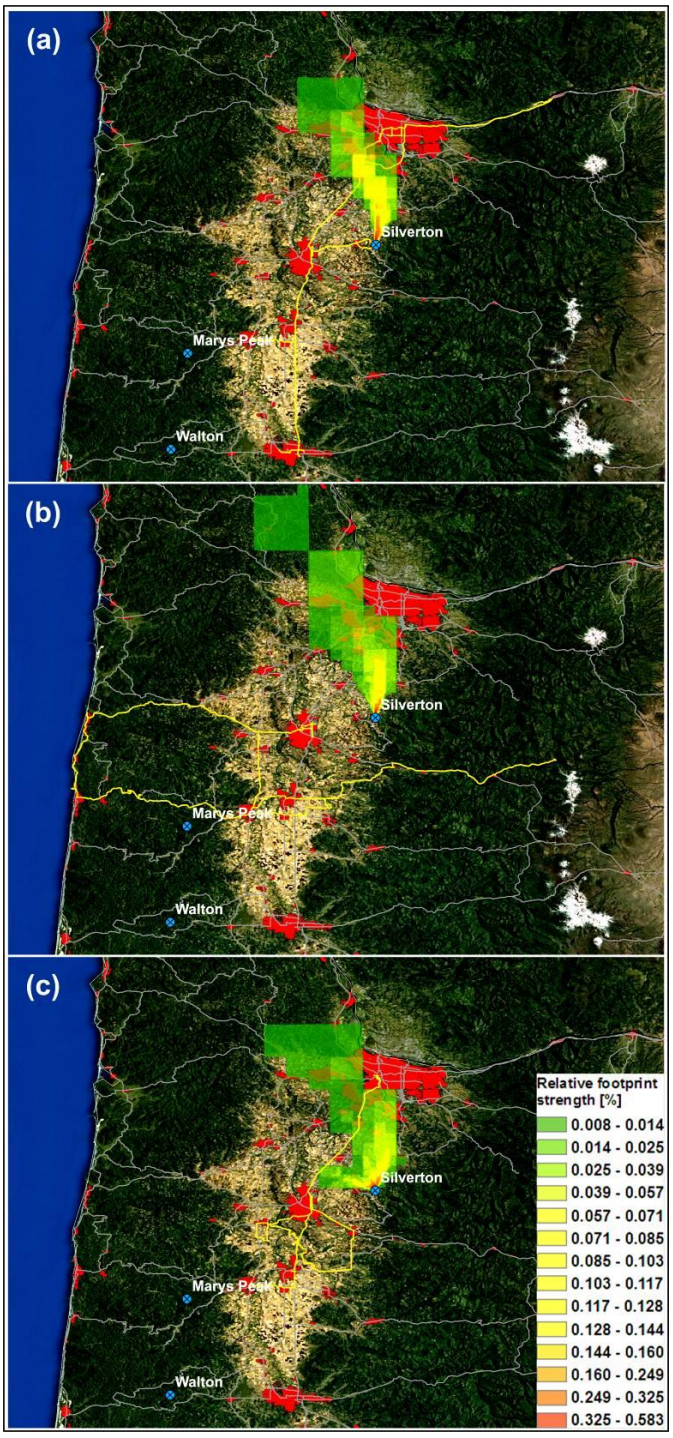

Figure 2: Tower locations and the daily footprint areas of the Silverton tower at 121 m above ground during the 3-day mobile campaign on July 10 (a), July 11 (b), and July 12 (c) 2012. The yellow lines show the routes driven during those days. The red areas show the locations of the urban centers. The classification of the relative strength of the footprints are defined by the Jenks natural breaks classification method and are cut off at 0.008% for the sake of visibility.

Geo-referenced road data was provided by the Oregon Department of Transportation, classified according to the Federal Functional Classification System (FFCS, US-DOT, 2013). The FFCS accounts for the type of usage of the roads and also incorporates information about the amount of traffic. The chemical composition of traffic emissions and therefore the $CO:CO_2$ emission ratios are highly correlated to the engine type and therefore vehicle type (e.g. McGaughey et al., 2004; Bishop & Stedman, 2008). Here we use the official vehicle classification system of the Federal Highway Administration (FHWA) of the US Department of Transportation (USDT, 2011).

3 Results and Discussion

3.1 Deriving traffic $CO:CO_2$ traffic emission ratios

To account for the different vehicle fleets and associated $CO:CO_2$ emission ratios on the roads while also accounting for the traffic amount and usage represented by the FFCS classification, we clustered the original FFCS road types based on the vehicle class distributions observed by ODT in 2011, into 3 final road type classes.

This was achieved by *k*-means clustering runs (e.g. Likas et al., 2003) using the frequency distributions of al vehicle classes, derived from the ODT traffic count information. The optimum cluster separation was reached by minimizing the Davies-Bouldin validity index (Davies and Bouldin, 1979). Cluster compositions were randomly changed and the number of classes consecutively increased until the maximum difference between the clusters was reached while the similarity of the vehicle distributions within each cluster was maximized.

For all final road type classes driven a weighted least-squares linear regression line through the origin was calculated with the intercept set to zero, the emission ratios are given by the slope values of the regression line.

Using the 3 final road classes, we calculated specific $CO:CO_2$ emission ratios over the route segments (Tab. 1).

Traffic counts conducted in 2011 over Oregon by the ODT indicate that, regardless of the road classes, the traffic on all roads in our study area are dominated by passenger

cars and other 2-axle/4-tire single unit vehicles (i.e. FHWA class 2 and 3, respectively). Nevertheless, the traffic composition differs in the amounts of the other vehicle classes (Fig. 3).

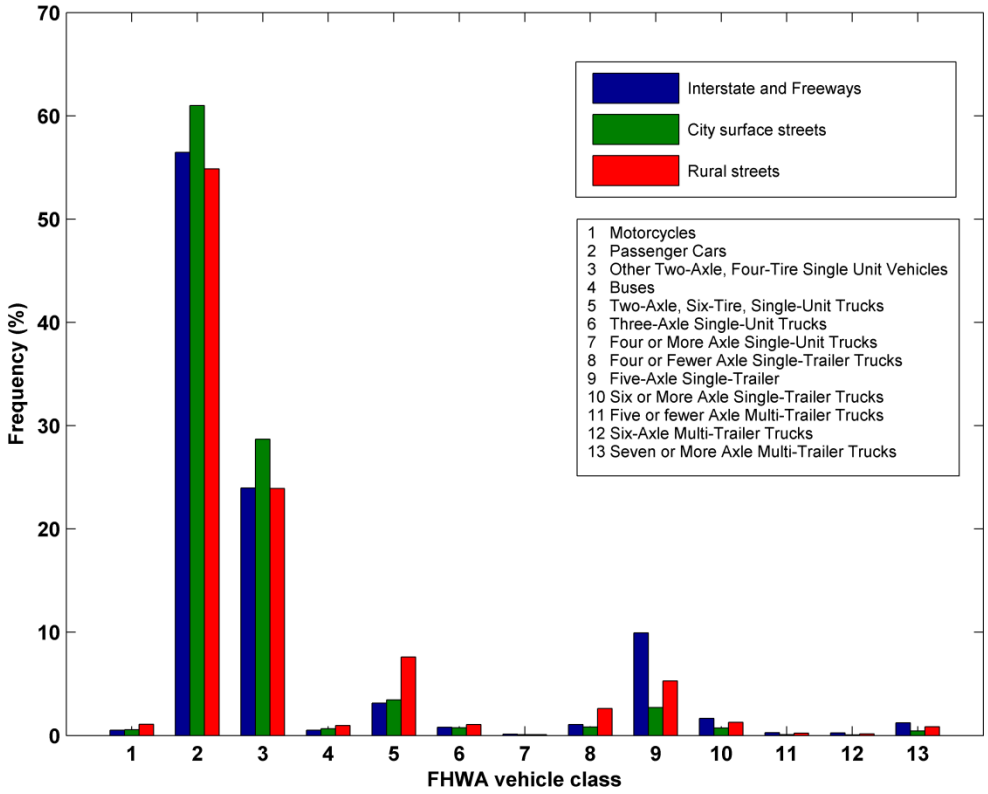

Figure 3: Frequency distribution of the 13 vehicle classes on the roads driven binned according to the 3 final road type classes used. The traffic data was provided by the Oregon Department of Transportation.

Ambient air samples always contain the signal of diurnal changes in CO_2 due to respiration and uptake of the surrounding biosphere. Furthermore they can be affected by changes in the background concentration due to long range transport. Thus, to determine CO:CO_2 emission ratios that are representative for the traffic emission only, the baseline levels of the two gases were removed by subtracting a varying baseline from the measured data (Fig. 4). Due to the continuously changing amount and composition of vehicles and associated emissions during the mobile on-road measurements the persistence intervals of temporal averages of CO and CO_2 mole fractions changed continuously and irregularly as well.

This makes a subtraction of a constant baseline unfeasible. Instead a moving-window analysis with a window width of 60 seconds was used to detect the changing baseline sections.

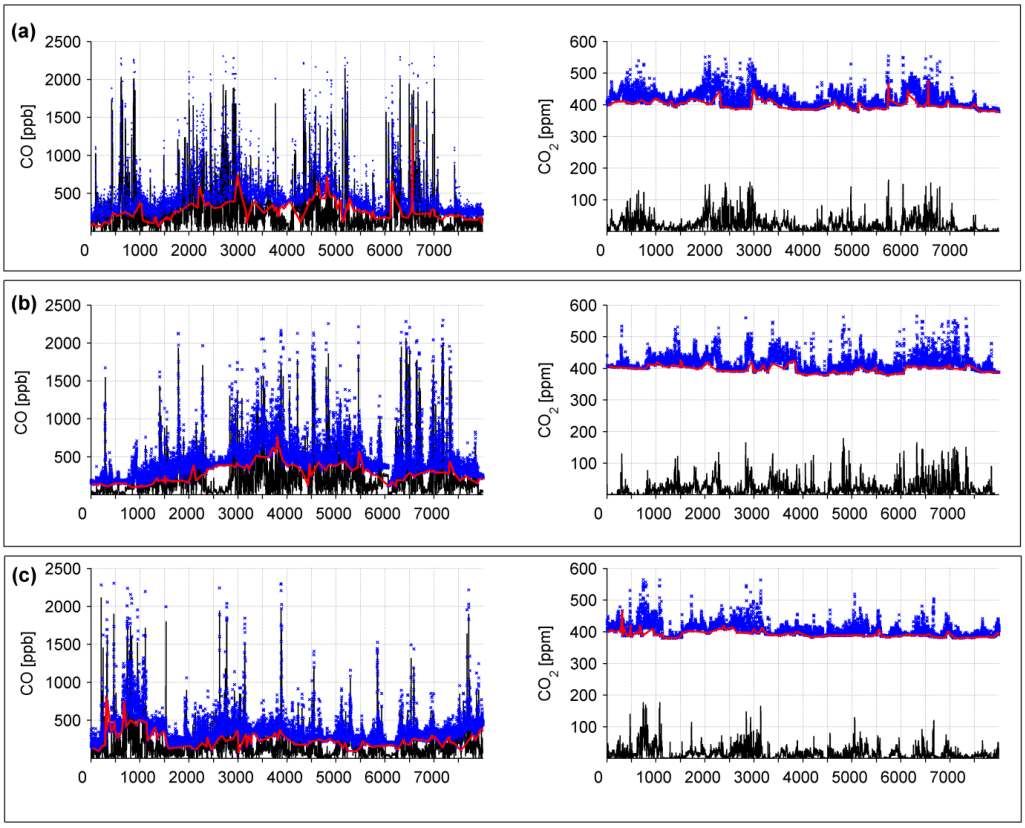

Figure 4: Sample of raw data (blue), sectional baselines (red), and excess values (black) of the mobile campaign for the road type classes 'Interstate and Freeways' (a) and 'City surface streets ' (b), and 'Rural streets' (c).

If the moving average mole fraction of CO or CO_2 changes by more than 2σ compared to the previous 60-second window values, a new baseline is defined for that section because the emissions and therefore the emission ratios change significantly. Furthermore, if the FFCS road types driven changed to FFCS road types that were not assigned to the same final road type class, the respective baseline section was ended too. This allows an objective and reproducible definition of the baselines that was found to work well for the on-road campaign driven (Fig. 4).

It is important to note that by this analysis, we are quantifying the excess CO and CO_2 above the local background.

The ratio of these quantities represents the weighted emission ratio for that section of road (i.e., the ratio of total CO emitted to the total CO_2 emitted), provided that there are no other sources contributing to the excess signal. By removing the time-varying background as we have, we restrict the excess to sources that are on or near the road.

The data of the mobile campaign was separated into 100 bins in excess carbon dioxide levels. To exclude values from further analyses that are mostly attributed to single point sources (i.e. very close vehicles), we removed continuous peak episodes of 5 seconds or less with values higher than 100 ppm above the CO_2 baseline. The linear regression coefficient R^2 drops significantly for excess values higher than 100 ppm CO_2 over the CO_2 baseline. Therefore, the applied restriction reduces the uncertainty of the derived emission ratios as the values are scattered over a wide range for those high values, reducing the goodness of fit for the regressions. Moreover, with increasing excess values the number of observations decreases with an exponential rate (Fig. 5), further increasing the standard error for the bin averages of rare excess values over 100 ppm.

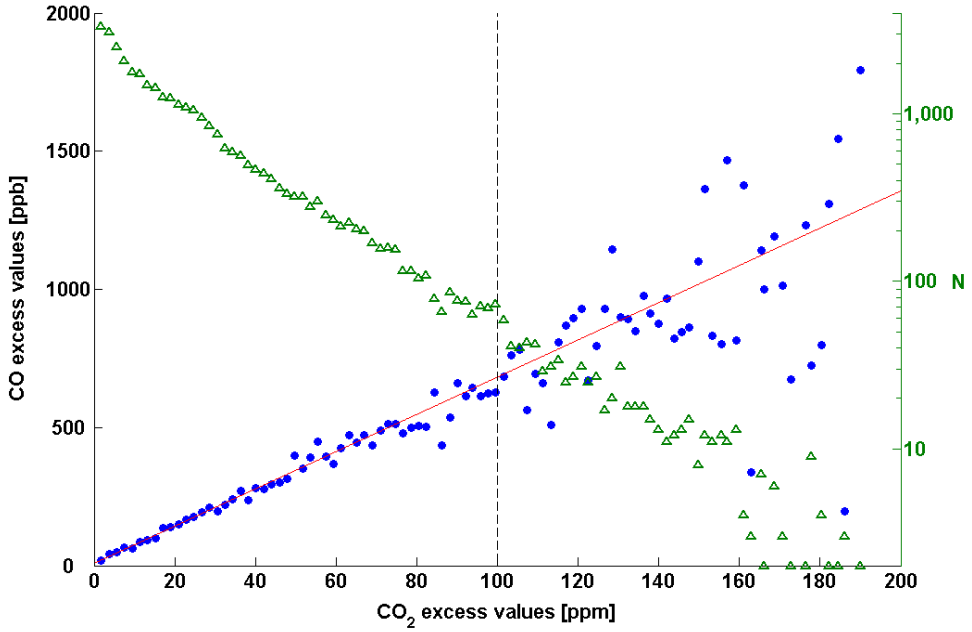

Figure 5: Scatterplot of the binned CO and CO_2 excess values measured during the 3-day campaign. The linear regression line (red) exhibits a regression coefficient R^2 of 0.97 for values limited to 100 ppm above the CO_2 excess line a (R^2 = 0.86 if all values are included). All regressions are calculated using a 95% confidence interval (p<=0.05). The number of observations per bin N is given by the green triangles on a logarithmic scale (green ordinate on the right).

The obtained emission ratios are shown in Table 1. The Rural streets exhibit a significantly lower emission ratio which most likely associated with the generally lower CO and CO_2 concentrations that can be found in those rural areas where the traffic density is much lower compared to the other road type classes as also indicated by the AADT value which is roughly only a quarter of the AADT of the other road type classes as observed during the ODT traffic count. The lower emission ratios observed for the rural roads may indeed be the case, but because of the substantially lower traffic density, and because the CO emissions can be skewed by a small number of high emitters, we may not have achieved a representative data set in this road type. Additional measurements would allow us to determine if emission ratio in rural areas is statistically different from the other road types.

Table 1: Specific emission ratios and uncertainties obtained during the on-road campaign. The AADT values given are averaged over all FFCS road types in the respective class. The uncertainties represent the bounds of the slope value of the fitted linear function with a 95% confidence interval.

Road type class	Incorporated FFCS road types	Emission ratio (ppb CO / ppm CO_2)	Uncertainty (ppb CO / ppm CO_2)	Mean AADT	Number of observations
Interstate and Freeways	Urban Interstate, Rural Interstate, Other Urban Freeways and Expressways	7.61	±1.50	11541	12182
City surface streets	Other Urban Principal Arterial, Urban Collector, Urban Local, Urban Minor Arterial	9.48	±2.15	12063	11306
Rural streets	Rural Local, Rural Major Collector, Rural Minor Arterial, Rural Minor Collector, Other Rural Principal Arterial	5.56	±1.78	3257	13606

The emission ratio measured on the city surface streets is the highest and exceeds the emission ratio measured on the Freeways and Interstates by 1.87 ppb CO per ppm CO_2. The city surface streets represent the urban areas where the traffic density is highest (Tab. 1). In addition, most cold starts occur in the urban areas. It is known that CO emissions from cars are highest during the first 5-10 km when the engine is still cold (e.g. Pokharel et al., 2003).

This leads to higher CO mole fractions and CO:CO_2 emission ratios, especially (but not limited to) during the rush hour times when the majority of people starts commuting. Another potential reason for the lower emission ratios found on the Interstate sections and Freeways is that Interstates and Freeways show a higher percentage of the heavy duty trucks of the vehicle class 6 (Fig. 3). The heavy trucks in that vehicle class are equipped with Diesel engines.

Diesel engines emit less CO than gasoline motors which are more common in the US even if the gasoline motors are equipped with catalytic converters. This potentially contributes to the lower CO:CO_2 emission ratios of this road type class.

The linear regressions were weighted according to the number of samples in the bins and the associated standard deviation to account for the uncertainty of the measurements during an averaging interval. Using this approach the residual of the weighted least-squares regression was calculated through,

$$S = \sum_i w_i \left(y_i - \hat{y}_i \right)^2, \quad (5)$$

with

$$w_i = \frac{N_i}{\sigma^2}. \quad (6)$$

Here, N_i gives the number of measurements in bin i, σ_i is the standard deviation over the CO samples y in bin i and $\hat{y}_i$ is the respective fitted value for the average of bin i. Hence, bin averages with lower variance and higher sample numbers will be weighted higher during the linear least-squares fit. S was minimized applying the Levenberg-Marquardt method (e.g. Moré, 1978).

A weighted total average of the emission ratios was calculated to obtain an average value that can directly be applied to the CO values measured at the Silverton tower. This result is an average emission ratio of 7.43 (± 1.80) ppb CO per ppm CO_2 for the fleet in our study area.

In Figure 6 we compare this result with studies of direct vehicle emission in several U.S. cities by Bishop and Stedman (2008) and Turnbull et al. (2011).

In those study, a range of CO:CO_2 emission ratio of 9 - 37 ppb CO per ppm CO_2 was found for the years 1997 through 2007. The conversion of units from gCO per kg fuel to ppm CO per ppm CO2 for the comparison was done according to Pokharel et al. (2001).

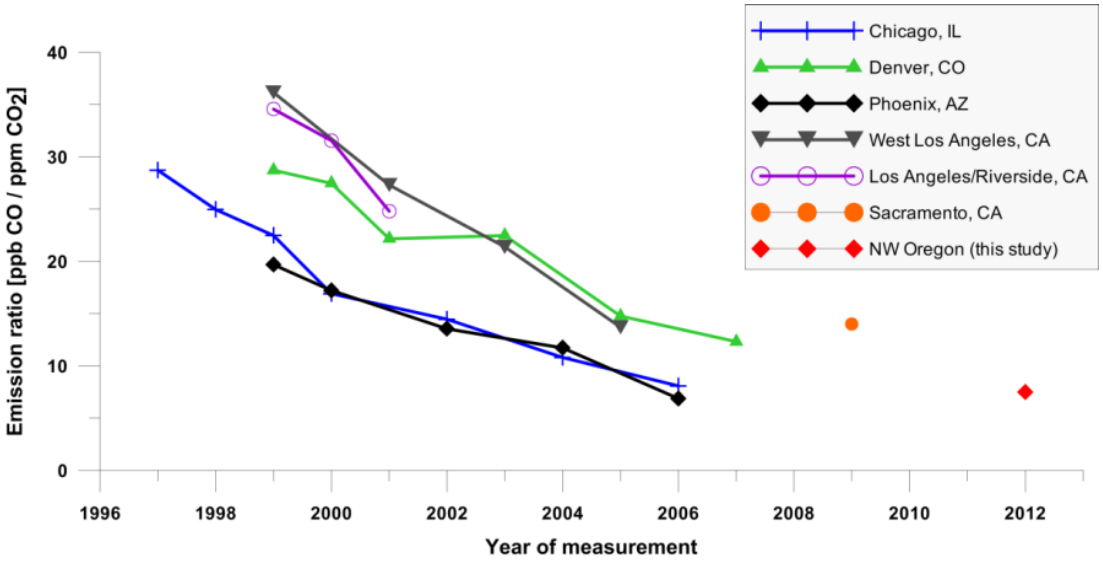

Figure 6: Extrapolation of the previous study results (Bishop & Stedman, 2008 and Turnbull et al., 2011). The continuing overall improvement in the emissions of the vehicle fleet in the United States (due especially to the retirement of older, more highly polluting vehicles) contributes to the overall reduction of the emission ratio with time.

The ratios in Bishop and Stedman (2008) are generally higher than the ratios shown in Tab. 1. However, the authors noted that the emission ratio highly depended on the age of the vehicle, and that in every city, the average emission ratio dropped significantly from year to year.

The observed average emission ratio of 7.43 ppb CO per ppm CO_2 is consistent with what can be expected from a vehicle fleet that is five years more modern than those studied in Bishop and Stedman (2008).

3.2 Correcting the CO_2 values of the tower data

The CO values measured at the Silverton tower are used to remove the traffic related traffic portion from the temporally corresponding CO_2 values by applying the road traffic specific CO:CO_2 emission ratio from the mobile measurements.

In Figure 7 the power spectra (Priestley, 1981) of the CO and CO_2 time series are shown. The spectra of all towers exhibit a clear 24-hour signal for CO_2 at all heights showing the diurnal run of the CO_2 uptake and release by vegetation (Fig. 7 b, d, and f). In opposition to that, a significant 24-hour peak (i.e. above the white-noise range, not shown) for CO, only occurs in the spectrum of the Silverton tower. As traffic from the surrounding urban areas and streets is the only regular and periodic source of CO, the spectral analysis clearly show the effect of daily fluctuations of the volume of traffic that affects the mole fractions (Fig. 7e).

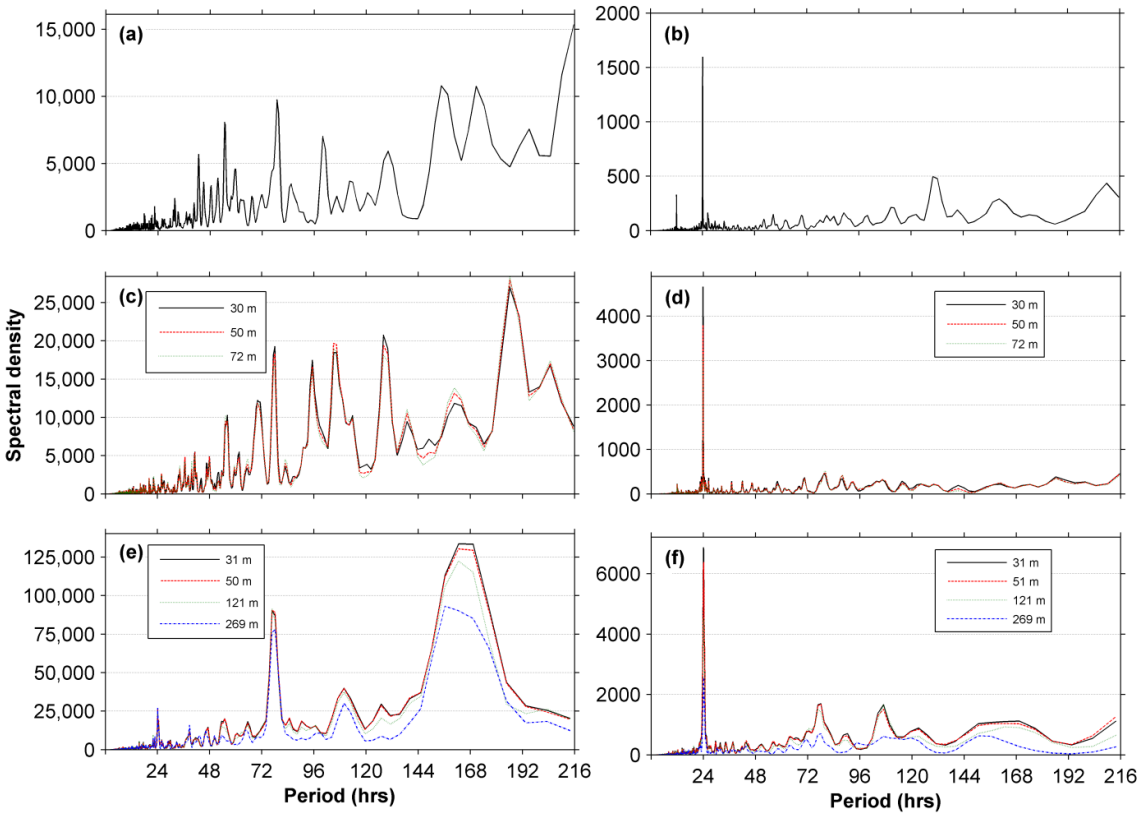

Figure 7: Spectral densities of the mole fraction time series of CO (left) and CO_2 (right) for the towers at Mary's Peak (1st row), Walton (2nd row) and Silverton (3rd row) for all inlet heights. The spectral density values were transformed using a Hamming filter function with a window width of 5.

An additional peak in the CO spectrum at the Silverton tower can be found at the 168 hour period. This corresponds to a weekly fluctuation showing the cyclic occurrence of the traffic influence that is reduced during the weekend.

At the rural towers at Mary's Peak and Walton (Fig 7 a and c) the weekly CO signal is less pronounced compared to the spectrum of the Silverton tower (Fig 7 e) presumably because the CO emitted through traffic is transported over longer distances to the towers and only during specific wind directions. In addition, the CO concentrations are strongly diluted by the time the air masses reach those sites in the forested Oregon Coast Range.

To evaluate the results from the decomposition approach we compared the remainders of the CO_2 (i.e. the values with the traffic emissions removed) with CO_2 values unaffected by traffic emissions and atmosphere-biosphere exchange during times when such background values where available at the Mary's Peak tower.

Because the air sampled at the Walton tower is transported over at least 86 km (straight line) before arriving at the Silverton tower the effects of uptake and release of CO_2 by the biosphere on the surface between the two towers during transport ($\Delta CO_{2\ biosphere}$) needs to be accounted for. Removing the $\Delta CO_{2\ biosphere}$ prior to the comparison allows a valid assessment of the performance of decomposition approach when applied to remove the traffic portion of the CO_2 signal. This was achieved by calculating the vertical CO_2 fluxes within the footprints of the Silverton tower with the Community Land Model (CLM 4.5). The Net Ecosystem Exchange (NEE) in µmol m^{-2} s^{-1} was calculated using a horizontal resolution of 1/24 degree. To prepare for climate input, historical meteorological data from *CMIP5* model *MIROC5* was downscaled from daily to sub-daily temporal resolution using multivariate adaptive constructed analogs method (Abatzoglou and Brown, 2012; Abatzoglou, 2013). The applied parameterization of plant functional types followed Hudiburg et al. (2013). Model parameters such as V_{cmax} and *FLNR* were obtained using A/C_i curves from the *LeafWeb* project (Sun et al., 2014). The land cover information was derived from the *NALCMS* dataset (NRCan/CCRS et al., 2013) with a spatial resolution of 250 m. The footprints for all 4 inlet heights at the Silverton tower were calculated with the WRF-STILT model setup as described in Göckede et al. (2010). To get the 4d meteorological fields used for the STILT (Stochastic Time-Inverted Lagrangian Transport) model (Nehrkorn et al., 2010), a horizontal resolution of 18 km was used for the outer grid and 6 km for the nested grid of the WRF (Weather Research and Forecasting, Ver. 3.5) model (e.g. Michalakes et al., 2001).

The footprint strength values calculated with STILT are given in ppm / (µmol m^{-2} s^{-1}) for each grid cell and can be used to calculate the change in mole fractions induced by the surface at a receptor location at a certain time (Lin et al., 2003). The number of particles released at the model receptor point (position of a tower inlet) for the backward trajectory calculation was set to 250. In Figure 8 the calculated *NEE* values for the area are shown including the intersecting footprint of the tower.

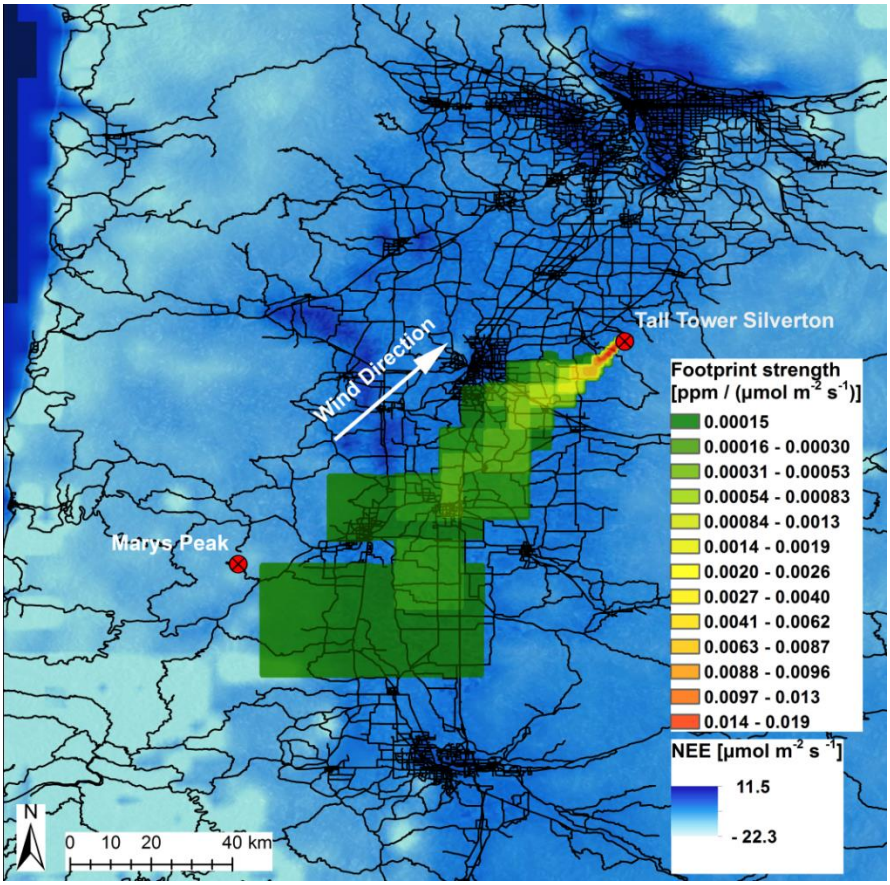

Figure 8: Net ecosystem exchange modeled with CLM 4.5 used to estimate the CO_2 added or removed by the biosphere during transport from the Mary's Peak tower. The example shows the fluxes during noontime and the footprint of the air sample inlet at 51 m above ground of the tall tower in Silverton for July 5, 2012.

Using the *NEE* flux estimates in combination with the WRF-STILT footprints strength *FS*, the changes in the mole fraction that are associated with the atmosphere-biosphere exchange can be directly calculated and subtracted from (or added to) the mole fractions measured at the tall tower in Silverton through,

$$\Delta CO_{2\ biosphere} = FS \cdot NEE\ . \qquad (7)$$

After the biosphere component is removed from the CO_2 signal, the traffic emissions are removed using the emission ratios *ER* in a second step.

Because excess values for the CO were used to derive the CO:CO_2 emission ratio, the baseline of the CO from the Silverton tower has to be removed too, in order to only leave the CO emission values that are superimposed on the measured total CO background mole fractions. The baseline was removed by subtracting the temporally corresponding CO concentration measured at the tower in Walton. The Walton tower was chosen to remove the baseline of the Silverton CO data because the Mary's Peak background tower used for the background CO_2 had significant gaps in the CO data series during the study period in 2012.

Since the Walton tower is also located in the vast fir forest of the Oregon Coast Range Mountains (Fig. 2) it is not affected by traffic-related CO emissions either. Hence, unlike the CO_2 mole fractions which show effects of uptake and release by the vegetation, the CO time series can directly be used as baseline level. Here, the CO from the uppermost inlet level at 72 m a. g. l. was chosen. However, with Pearson correlation coefficients ranging from 0.98 to 0.99, the correlations between the time series of all 3 levels are very high indicating that the CO time series from all measurement heights are equally suitable as background CO signal.

The traffic portion of the CO_2 at the Silverton tower is then calculated through,

$$\Delta CO_{2\ traffic} = \frac{CO_{excess} \cdot f}{ER}\ , \tag{9}$$

with

$$CO_{excess} = CO_{measured} - CO_{baseline}\ , \tag{10}$$

where $CO_{measured}$ gives the CO mole fraction at the Silverton tower, $CO_{baseline}$ the corresponding CO measured at the Walton tower, and *ER* is the average traffic CO:CO_2 emission ratio. A scaling factor *f* is applied to account for the fact that not all CO measured at the Silverton tower originates from traffic.

Portions are also transported over larger regions or emitted by other local sources such as non-traffic fuel combustion, industrial processes, or fires. Since 86% of atmospheric CO in Oregon originates from on-road traffic (US-EPA, 2013) the factor *f* is set to 0.86, accordingly.

The final remainder of CO_2 at the Silverton tower is then given by:

$$CO_{2\ background} = CO_{2\ measured} - \Delta CO_{2\ biosphere} - \Delta CO_{2\ traffic}\ . \qquad (11)$$

The adjusted $CO_{2\ background}$ mole fractions are then compared to the measured background values from the Mary's Peak tower.

3.2.1 Comparison of directly measured background tower data and the adjusted urban tower data

Using the results from the WRF-STILT trajectories and footprint analyses for the Mary's Peak tower, only mole fractions measured at times with practically no surface exchange were extracted. We chose segments of the hourly measured time series with temporally associated footprint strength values of < 0.01 ppm / (µmol m^{-2} s^{-1}) summarized over the entire footprint area.

In a second step we analyzed the correlation between the CO_2 mole fractions measured at Mary's peak tower and the highest inlet of the Walton tower at 72 m above ground.

For the complete time series the Pearson correlation between the CO_2 time series of the two towers is high with r = 0.86 on a 99% confidence level ($p < 0.01$) showing the similarity of the two sites during most times. Using a moving window with a 12 hour window width, the Pearson correlations between the sections of the CO_2 mole fractions at the two towers were calculated.

During times with stable conditions when the Mary's Peak tower is decoupled from the surface-atmosphere exchange processes in the boundary-layer the correlation between the CO_2 mole fractions at the two towers drops significantly (Fig. 9).

For the final comparison of the tower baseline values derived using the correlations between the measurements at the tower on Mary's Peak and in Walton and the baseline values that were obtained using the decomposition approach for the Silverton tower we only used data that met the following three criteria.

First, only data intervals with surface influence values integrated over the footprint area of the Marys' Peak tower of less than 0.01 ppm/ (µmol m-2 sec-1) were considered. Secondly, only data intervals that exhibit an r^2 of less than 0.1 ($p \leq 0.05$) using a 12 hour moving window for the Mary's Peak tower and the Walton tower (72 m inlet height) were used.

Thirdly, only data intervals with south-westerly or westerly wind directions between 200 and 270 degrees over at least 3 hours were used to simply assure a physical correlation between the air masses measured at the Mary's Peak tower and the Silverton tower considering their relative geographic locations (Fig. 2).

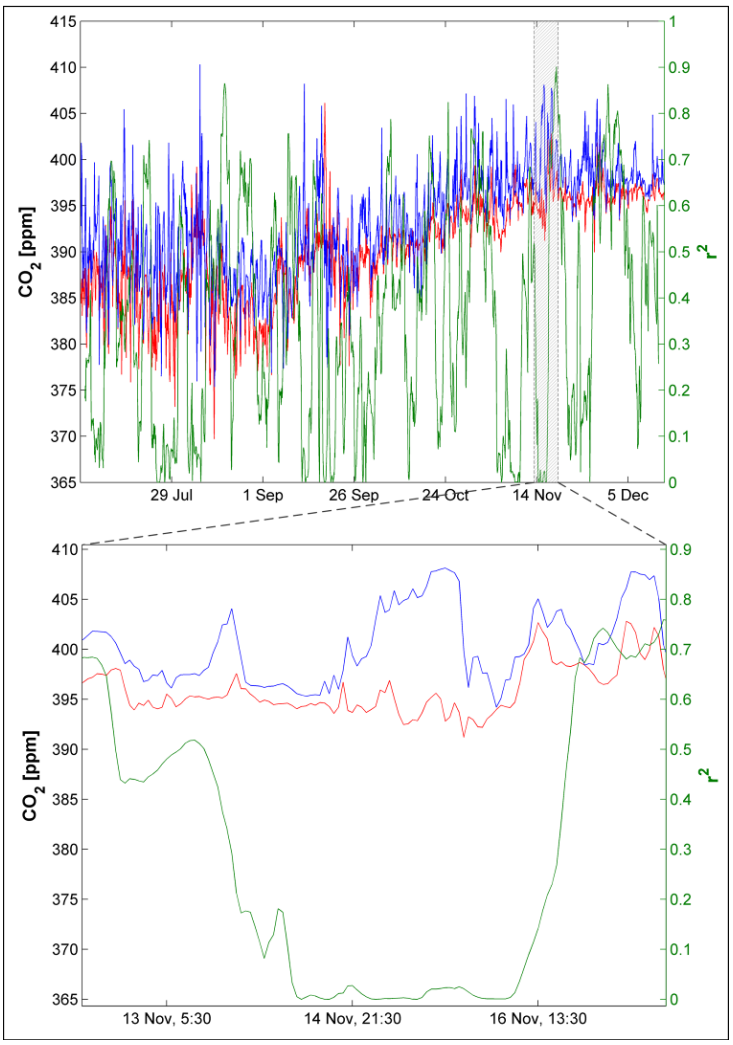

Figure 9: CO_2 mole fractions at the Walton tower (72 m inlet, red line) and the Mary's Peak tower (blue line). The green line shows the squared values of the Pearson correlation for the 24-hour moving window intervals. Time is given in UTC.

Due to the seasonal significant changes of CO emissions through heating in populated areas and therefore changes in the CO:CO_2 ratios through sources unrelated to traffic during the colder seasons (heating in urban areas), we limited the application of the emission ratios obtained in summer to the summer period only and stopped at the end of September.

During summer when the measurements were conducted, the anthropogenic emissions of CO and CO_2 in the Willamette Valley are dominated by the transit sector and the measurements and analyses are unbiased through other significant heating emissions with changing CO:CO_2 emission ratios to the greatest possible extent.

On average, the CO_2 mole fractions at the Silverton tower were reduced by 2.56 ppm (σ=2.01 ppm) for the measurement closest to the surface at 31 m above ground. The CO_2 mole fractions for the other heights were on average reduced by 2.56 ppm (σ=2.02 ppm, 52 m), 2.43 ppm (σ=1.98 ppm, 121 m), and 2.23 ppm (σ=1.96 ppm) for 269 m above ground.

Figure 10 shows the result of the comparison between the CO_2 values derived by background measurements above the boundary layer during stable conditions at Mary's Peak tower and the decomposition of the Silverton CO_2 signal through application of the emission ratios, respectively. The increased correlations after the two decomposition steps are clearly visible. The correlations between the measured background values and the final decomposed CO_2 values for the 4 heights at the Silverton tower are all very high and range between 0.61 and 0.93 ($p < 0.05$).

The overall uncertainty for the correction method presented has to be accounted for when using the corrected data in particular for methods that are highly sensitive to uncertainties of the input data such as inverse modeling. The total uncertainty of the corrected mole fractions comprises the uncertainty of the CO values while applied according to Eqs. 9 and 10 (7.50 ppb), the uncertainties of the applied average traffic emission ratio (1.80 ppb/ppm), and the measurement uncertainty for CO_2 as described in section 2.3 (0.18(4) ppm).

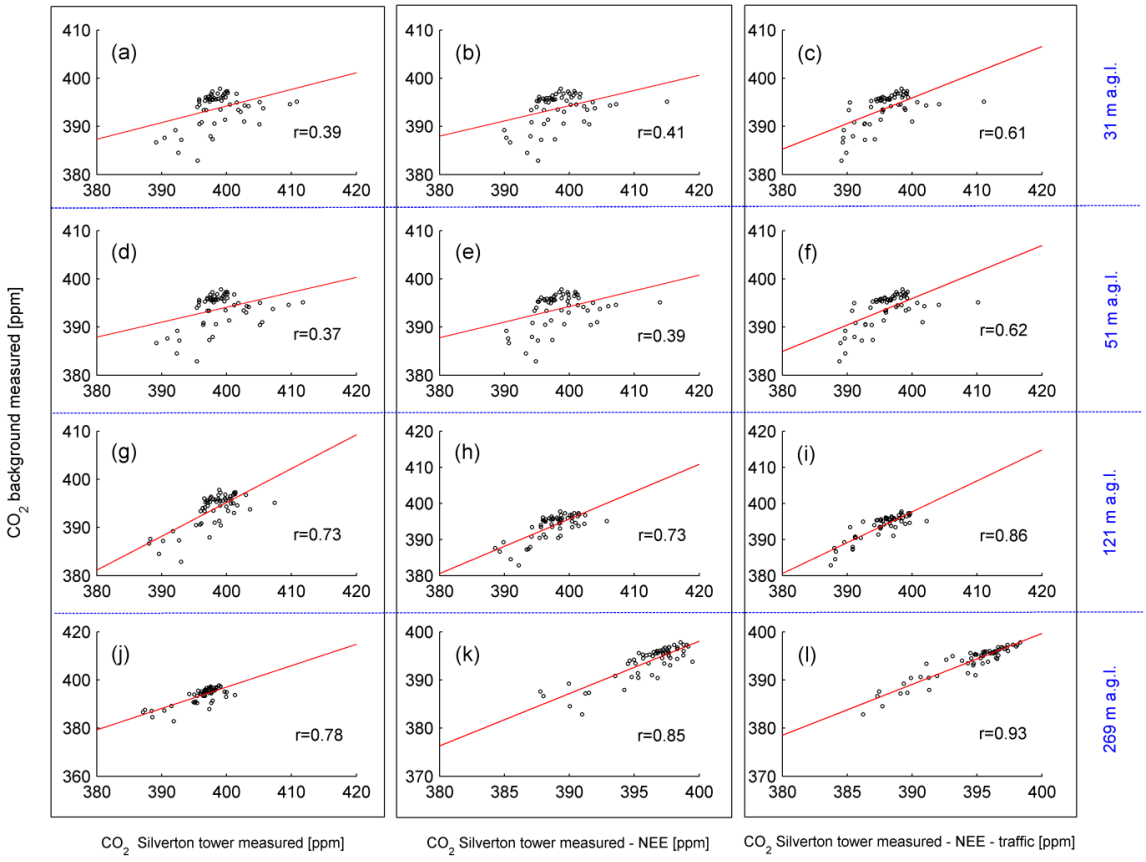

Figure 10: Linear regression results for the excess mole fractions obtained using measured background at the Mary's Peak tower and the CO_2 measurements of the Silverton tower measurements. The regressions shows the increasing similarity and correlation between the measured background and the calculated background at the Silverton tower for the raw, measured values (left column), after removing the biosphere component in a first step (middle column), and after the additional removal of the traffic component in a second step (right column) for all 4 inlet heights.

Hence, to account for the additional error term for the uncertainty induced by the usage of the CO excess values, we accumulated the partial derivatives of Eq. 9 using the general error propagation. Using the partial derivatives for the product in Eq. 9 the relative uncertainty for $\Delta CO_{2\ traffic}$ is calculated through:

$$\delta\Delta CO_{2\ traffic} = \left(\left(\frac{\delta CO_{excess}}{\overline{CO}_{excess}} \right)^2 + \left(\frac{\delta ER}{\overline{ER}} \right)^2 \right)^{1/2}, \qquad (12)$$

where δ indicates the absolute uncertainty of the respective incorporated variable and the overlines denote the average of that variable.

We calculated the average of the excess values for the entire study period for the data series of all 4 inlet heights used. The average CO excess values for the study period ranged between 18.402 and 22.158, depending on the inlet height, and averaged 20.908 ppb. According to Eq. 12 the percentage uncertainty of for $\Delta CO_{2\ traffic}$ caused by the uncertainty of the emission ratio and the uncertainty of the CO values used is 43%.

To obtain an absolute uncertainty value for $\Delta CO_{2\ traffic}$ we used the highest average $\Delta CO_{2\ traffic}$ of 2.56 ppm found at the Silverton tower for the analyzed period to obtain a conservative estimate for the total uncertainty. The corrected CO_2 mole fractions are then calculated by subtracting the $\Delta CO_{2\ traffic}$ (Eq. 9) from the CO_2 mole fraction measured at the tower (Eq. 10).

Therefore, another error propagation step is needed to obtain the total uncertainty by adding the measurement uncertainty of the tower values and the uncertainty of the subtrahend ($\Delta CO_{2\ traffic}$). Using simple error propagation, the total uncertainty for the corrected CO_2 tower values with the traffic emissions removed is ±1.04 ppm.
The uncertainty added to the initial measurement uncertainty for CO_2 at the tower by the decomposition algorithm (0.86 ppm) is considered an improvement compared to the application of uncorrected CO_2 mole fractions. In comparison, the traffic portion of CO_2 exhibits maximum values of 11.9 ppm during summer 2012 for the two lowest heights. Thus, a much larger uncertainty needs to be considered if the uncorrected CO_2 mole fractions affected by traffic emissions are directly used to inverse model the uptake and release of CO_2 by the biosphere.

After calculating the traffic related portion of CO_2 with the approach presented the hourly $\Delta CO_{2\ traffic}$ values were separated into measurements on weekdays and measurements on weekends or holidays. The diurnal cycles differ significantly for weekends and weekdays (Fig. 11). A peak in the morning hours (8h local time) can be observed in panel during regular weekdays. This is associated with the first rush hour traffic which occurs in the morning hours between 6 and 9. As opposed to measurements within cities or tunnels (e.g. McGaughey et al., 2004; Lavaux et al., 2013) the rush hour peaks are less pronounced in the tower measurements presented.

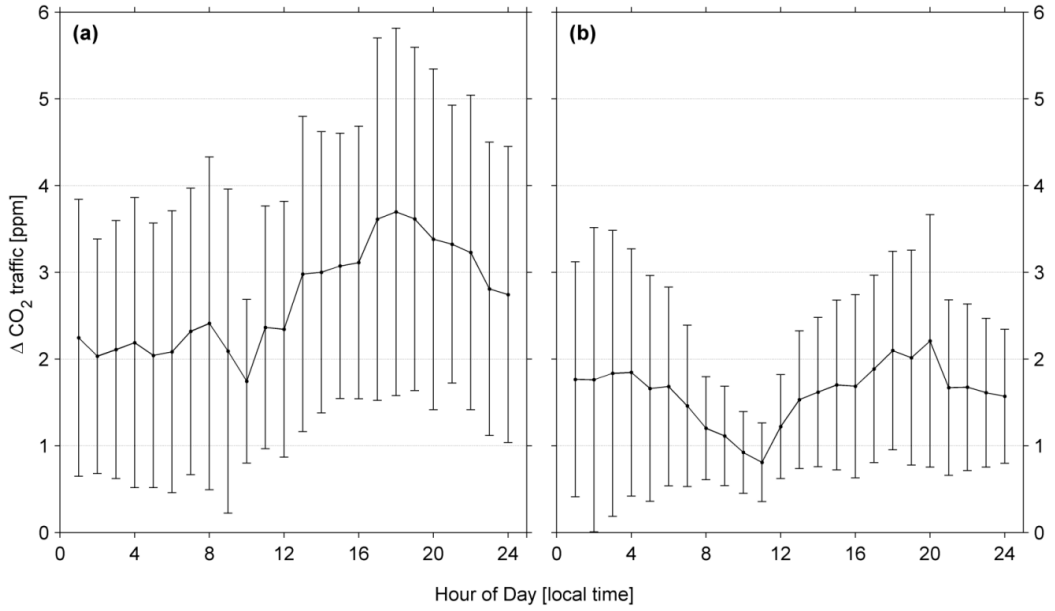

Figure 11: Diurnal cycle of the derived $\Delta CO_{2\ traffic}$ for the Silverton tower (121 m inlet) during summer 2012 separated into weekdays (a) and weekends (b). The error bars indicate the 1σ range of the hourly values averaged for the corresponding hour of the day.

This is due to the fact that the Silverton tower does not directly represent a specific city or tunnel but rather gets the integrated emissions from urban areas and road network in the larger footprint area. This is associated with a propagation delay and dispersion bringing the gas from the urban centers and major roads in the Willamette Valley (Fig. 2) to the tower location in Silverton. Considering the distances to potential source areas and the tower, a moderate wind will take 2-3 hours to bring the signal to the tower leading to the accumulation effect of $\Delta CO_{2\ traffic}$ noticeable in both panels of Figure 11.

The calculated traffic related portion of CO_2 is overall lower on weekends and holidays (daily average = 1.61 ppm) compared to the weekday emissions (daily average = 2.69 ppm). This also applies to the diurnal variation of the hourly average traffic CO_2 emissions as shown in Figure 11(b). The weekdays exhibit a minimum of 1.74 ppm and a maximum of 3.71 whereas on weekends the values of $\Delta CO_{2\ traffic}$ range between a minimum of 0.81 ppm and a maximum of 2.21 ppm.

4 Conclusion

The application of CO:CO_2 emission ratios obtained through mobile campaigns that cover representative areas of a tower's footprints provide a useful method to remove the traffic portion of CO_2 time series. We highlight the flexibility of this methodology; in a short campaign, we were able to quantify the CO:CO_2 emission ratio over a variety of different road types at different grades and traffic conditions. Campaigns which rely on tunnel accumulation (McGaughey et al., 2004; Popa et al., 2014) or direct tailpipe emissions (Bishop and Stedman, 2008) are always more limited in the road types, traffic conditions, and road grades that can be quantified.

Unlike previous studies of CO:CO_2 emission ratios that were used to assess the amount of CO_2 from traffic, our measurements and analyses aim to represent a larger area rather than a distinct city. The mole fractions measured at the main tower (Silverton, OR) do not only represent one distinct city but a valley area of more than 14000 km^2, including several urban centers and the associated road network.

Moreover, the emission ratios presented are not derived from tower data but from independent mobile in-situ measurements covering a significant portion northwest Oregon. CO and CO_2 mole fractions where sampled on the roads where they are released allowing a more direct calculation of the emission ratio without unwanted effects of dilution and other issues that occur when the sample is transported over a larger range before reaching the measurement instrument (e.g. Sun et al., 2007).

It is mentioned here that the approach presented in this study focuses on the traffic related emissions of CO_2 that pose the biggest problem due to their temporal and spatial variability and their strong dominance in the study area.

Emissions from significant, single sources such as power plants with continuous well localized emissions can be considered using inventory information. In combination with proper footprint analyses the effect of such well localized sources can easily be considered as opposed to fluctuating traffic emissions.

Our results are limited to the summer months represented by data collected during the mobile campaign. For future applications more mobile campaigns are recommended to cover the seasonality of the CO:CO_2 emission ratios.

However, residential heating as part of other fuel combustion processes during fall and winter produces emissions with significantly lower CO:CO_2 emission ratios compared to the traffic emissions, reaching from 0.24 to 3.3 ppb CO / ppm CO_2 (Vogel et al., 2010). With relatively low CO emissions these sources are hardly detectable through tower CO observations if the tower is not located in the immediate vicinity of such sources. A more important reason for additional driving campaigns are the extended cold start times for passenger vehicles as discussed in section 3.1. Significantly lower ambient temperatures will potentially increase the warm-up times for engines which extends the time with higher CO:CO_2 emission ratios from vehicles in winter.

The corrected mole fractions of the observation tower mitigate the bias of modeled uptake and release of CO_2 by the biosphere towards CO_2 mole fractions temporally elevated by traffic emissions. With respect to inverse modeling approaches the increase of the uncertainty of the corrected CO_2 mole fractions could be kept relatively small with an additional 0.86 ppm for the study period.

Acknowledgements

This research was supported by the NOAA Earth System Science Program (Grant no. NOAA-OAR-CPO-2012-2003041). The authors also would like to thank David Rupp for his assistance with the down scaling of the climate input data for the CLM runs.

References

Abatzoglou, J.T, and Brown, T.J.: A Comparison of Statistical Downscaling Methods Suited for Wildfire Applications, Int. J. Climatol. 32, 772-780, 2012.

Abatzoglou, J. T.: Development of gridded surface meteorological data for ecological applications and modelling, Int. J. Climatol. 33, 121-131, 2013.

Bergeron, O., Strachan, I.B.: CO_2 sources and sinks in urban and suburban areas of a northern mid-latitude city, Atmos. Environ. 45, 1564-1573, 2011.

Bishop, G. and Stedman, G.: A decade of on-road emissions measurements. Environ. Sci. Technol., 42, 1651-1656, 2008.

Brasseur, G.P., Prinn, R.G., Pszenny, A.A.P. (eds.): Atmospheric Chemistry in a Changing World. An Integration and Synthesis of a Decade of Tropospheric Chemistry Research, Springer, Berlin, Heidelberg, New York, 300 pp., 2003.

Chen, H., Winderlich, J., Gerbig, C., Hoefer, A., Rella, C. W., Crosson, E. R., Van Pelt, A. D., Steinbach, J., Kolle, O., Beck, V., Daube, B. C., Gottlieb, E. W., Chow, V. Y., Santoni, G. W., and Wofsy, S. C.: High-accuracy continuous airborne measurements of greenhouse gases (CO_2 and CH_4) using the cavity ring-down spectroscopy (CRDS) technique, Atmos. Meas. Tech., 3, 375-386, 2010.

Chen, H., Karion, A., Rella, C.W., Winderlich, J., Gerbig, C., Filges, A., Newberger, T., Sweeney, C., and Tans, P.P.: Accurate measurements of carbon monoxide in humid air using the cavity ring-down spectroscopy (CRDS) technique, Atmos. Meas. Tech., 6, 1031-1040, 2013.

Crosson, E. R.: A cavity ring-down analyzer for measuring atmospheric levels of methane, carbon dioxide, and water vapour. Appl. Phys. B92, 403-408, 2008.

Davies, D.L. and Bouldin D.W.: A cluster separation measure, IEEE Trans. Pattern Anal. Mach. Intell., 1 (1979), 224–227.

Finlayson-Pitts, B.J. and Pitts, J.N.: Chemistry of the Upper and Lower Atmosphere, Academic Press, San Diego, California, USA, 969 pp., 2000.

Fogg, P.G.T. and Sangster, J.M. (eds.): Chemicals in the Atmosphere - Solubility, Sources and Reactivity, John Wiley, Chichester, UK, 453 pp., 2003.

Friedlingstein, P., Houghton, R.A., Marland, G., Hackler, J., Boden, T.A., Conway, T.J. Canadell, J.G., Raupach, M.R., Ciais, P., and Le Quéré, C.: Update on CO_2 emissions, Nat. Geosc., 3,811–812, 2010.

Göckede, M., Michalak, A.M., Vickers, D., Turner, D.P., Law, B.E.: Atmospheric inverse modeling to constrain regional scale CO_2 budgets at high spatial and temporal resolution. J. Geophys. Res., 115, D15113, 2010.

Granier, C., Pétron, G., Müller, J.-F, Brasseur, G.: The impact of natural and anthropogenic hydrocarbons on the tropospheric budget of carbon monoxide, Atmos. Environ., 34, 5255–5270, 2000.

Gurney, K.R., Mendoza, D.L., Zhou, Y., Fischer, M.L., Miller, C.C., Geethakumar, S., and De la Rue du Can, S.: High Resolution Fossil Fuel Combustion CO_2 Emission Fluxes for the United States, Environ. Sci. Technol., 43, 5535-5541, 2009.

Hudiburg, T.W., Law, B.E., Thornton, P.E.: Evaluation and improvement of the Community Land Model (CLM 4.0) in Oregon forests. Biogeosciences 10: 453-470, 2013.

IPCC: Climate Change 2013: The Physical Science Basis. Contribution of Working Group I to the Fifth Assessment Report of the Intergovernmental Panel on Climate Change [Stocker, T.F., D. Qin, G.-K. Plattner, M. Tignor, S.K. Allen, J. Boschung, A. Nauels, Y. Xia, V. Bex and P.M. Midgley(eds.)]. Cambridge University Press, Cambridge, United Kingdom and New York, NY, USA, 1535 pp., 2013.

LaFranchi, B. W., Pétron, G., Miller, J. B., Lehman, S. J., Andrews, A. E., Dlugokencky, E. J., Hall, B., Miller, B. R., Montzka, S. A., Neff, W., Novelli, P. C., Sweeney, C., Turnbull, J. C., Wolfe, D. E., Tans, P. P., Gurney, K. R., and Guilderson, T. P.: Constraints on emissions of carbon monoxide, methane, and a suite of hydrocarbons in the Colorado Front Range using observations of $^{14}CO_2$, Atmos. Chem. Phys., 13, 11101-11120, 2013.

Lauvaux, T. et al.: Urban Emissions of CO_2 from Davos, Switzerland: The First Real-Time Monitoring System Using an Atmospheric Inversion Technique, J. Appl. Meteor. Climatol., 52, 2654-2668, 2013.

Likas, A., Vlassis, N., Verbeek, J.J.: The global k-means clustering algorithm, Pattern Recogn., 36, 451-461, 2003.

Lin, J.C., Gerbig, C., Wofsy, S.C., Andrews, A.E., Daube, B.C., Davis, K.J., Grainger, C.A.: A near-field tool for simulating the upstream influence of atmospheric observations: the stochastic time-inverted Lagrangian transport (STILT) model. J. Geophys. Res., 108, 4493.doi:10.1029/2002JD003161, 2003.

McGaughey, G.R., Desai, N.R., Allen, D.T., Seila, R.L., Lonneman, W.A., Fraser, M.P., Harley, R.A., Pollack, A. K., Ivy, J.M., Price, J. H.: Analysis of motor vehicle emissions in a Houston tunnel during the Texas Air Quality Study 2000, Findings from EPA's Particulate Matter Supersites Program, Atmos. Environ. 38, 3363-3372, 2004.

Michalakes, J., Chen, S., Dudhia, J., Hart, L., Klemp, J., Middlecoff, J., Skamarock, W.: Development of a Next Generation Regional Weather Research and Forecast Model. Developments in Teracomputing: Proceedings of the Ninth ECMWF Workshop on the Use of High Performance Computing in Meteorology. Walter Zwieflhofer and Norbert Kreitz (Eds.), World Scientific, Singapore, pp. 269-276, 2001.

Moré, J.J. The Levenberg-Marquardt algorithm: Implementation and theory, Lect. Notes Math., 630, 105-116, 1978.

Nehrkorn, T., Eluszkiewicz, J., Wofsy, S.C., Lin, J.C., Gerbig, C., Longo, M., and Freitas, S.: Coupled Weather Research and Forecasting--Stochastic Time-Inverted Lagrangian Transport (WRF-STILT) Model, Meteorol. Atmos. Phys., 107, 51-64, 2010.

NOAA ESRL: Global monitoring division: WMO/IAEA Round Robin Comparison Experiment - Archived Results, http://www.esrl.noaa.gov/ gmd/ccgg/wmorr/ results.php? rr=rr5&param=co2&group=group2, accessed online December 20, 2013, 2012.

NRCan/CCRS, USGS, INEGI, CONABIO and CONAFOR: The 2005 North American Land Cover at 250 m spatial resolution. Produced by Natural Resources Canada/Canadian Center for Remote Sensing (NRCan/CCRS), United States Geological Survey (USGS); Insituto Nacional de Estadística y Geografía (INEGI), Comisión Nacional para el Conocimiento y Uso de la Biodiversidad (CONABIO) and Comisión Nacional Forestal (CONAFOR), accessed online June 3, 2013 at http://landcover.usgs.gov/nalcms.php, published 2013.

Oda, T. and Maksyutov, S.: A very high-resolution (1 km × 1 km) global fossil fuel CO_2 emission inventory derived using a point source database and satellite observations of nighttime lights Atmos. Chem. Phys., 11, 543-556, 2011.

ODT (Oregon Department of Transportation): Background Report: The Status of Oregon Greenhouse Gas Emissions and Analysis, ODT Transportation Planning Analysis Unit, Salem, OR, USA, 46 pp., 2009.

ODT (Oregon Department of Transportation), Transportation Data Section, downloaded from http://www.oregon.gov/ODOT/TD/TDATA/tsm/docs/ Flow_Map_2011.pdf, accessed online 2 January, 2014.

Peters, W. Jacobson, A.R., Sweeney, C., Andrews, A.E., Conway, T.J., Masarie, K., Miller, J.B., Bruhwiler, L.M.P., Pétron, G., Hirsch, A.I., Worthy, D.E.J., van der Werf, G.R., Randerson, J.T., Wennberg, P.O., Krol, M.C., Tans, P.P.: An atmospheric perspective on North American carbon dioxide exchange: CarbonTracker, PNAS, 104, 18925-18930, 2007.

Peters, G.P., Marland, G., Le Quéré, C., Boden, T., Canadell, J.G., and Raupach M.R.: Rapid growth in CO_2 emissions after the 2008-2009 global financial crisis, Nat. climate change 2, 2-4, 2012.

Pillai, D., Gerbig, C., Ahmadov, R., Rödenbeck, C., Kretschmer, R., Koch, T., Thompson, R., Neininger, B., and Lavrié, J. V.: High-resolution simulations of atmospheric CO_2 over complex terrain – representing the Ochsenkopf mountain tall tower, Atmos. Chem. Phys., 11, 7445-7464, doi:10.5194/acp-11-7445-2011, 2011.

Pokharel, S.S.., Bishop, G.A., Stedman D.H.: Fuel-Based On-Road Motor Vehicle Emissions Inventory for the Denver Metropolitan Area, 10th International Emission Inventory Conference, Denver, CO, May 1-3, 2001.

Pokharel, S.S., Bishop, G.A., Stedman D.H., and Slott, R: Emissions Reductions as a Result of Automobile Improvement, Environ. Sci. Technol., 37:5097-5101, 2003.

Popa, M. E., Vollmer, M. K., Jordan, A., Brand, W. A., Pathirana, S. L., Rothe, M., and Röckmann, T.: Vehicle emissions of greenhouse gases and related tracers from a tunnel study: CO : CO_2, N_2O : CO_2, CH_4 : CO_2, O_2 : CO_2 ratios, and the stable isotopes ^{13}C and ^{18}O in CO_2 and CO, Atmos. Chem. Phys., 14, 2105-2123, 2014.

Priestley M. B.: Spectral Analysis and Time Series, 1st Ed., Probability and mathematical statistics, Vol. 1 and 2, Academic Press, London, 890 pp., 1981.

Rella, C. W., Chen, H., Andrews, A. E., Filges, A., Gerbig, C., Hatakka, J., Karion, A., Miles, N. L., Richardson, S. J., Steinbacher, M., Sweeney, C., Wastine, B., and Zellweger, C.: High accuracy measurements of dry mole fractions of carbon dioxide and methane in humid air, Atmos. Meas. Tech., 6, 837-860, 2013.

Seinfeld, J. H. and Pandis, S. N.: Atmospheric Chemistry and Physics: From Air Pollution to Climate Change, 2nd Edition, J. Wiley, New York, 1232 pp., 2006.

Strong, C., Stwertka, C., Bowling, D.R., Stephens, B.B., and Ehleringer, J.R.: Urban carbon dioxide cycles within the Salt Lake Valley: A multiple-box model validated by observations, J. Geophys. Res., 116, D15307, 2011.

Sun, J., Burns S.P., Delany A.C. et al.: CO_2 transport over complex terrain, Agr. Forest Meteorol., 145, 1-21, 2007.

Sun Y., Gu, L., Dickinson, R.E., et al.: Asymmetrical effects of mesophyll conductance on fundamental photosynthetic parameters and their relationships estimated from leaf gas exchange measurements, Plant Cell Environ. 37, 978-994, 2014.

Tans. P., Zhao, C. , Kitzis, D.: The WMO Mole Fraction Scales for CO_2 and other greenhouse gases, and uncertainty of the atmospheric measurements. 15th WMO/IAEA Meeting of Experts on Carbon Dioxide, Other Greenhouse Gases, and Related Tracer Measurement Techniques, Jena, Germany, September 7-10, 2009.

Turnbull, J. C., Karion, A., Fischer, M. L., Faloona, I., Guilderson, T., Lehman, S. J., Miller, B. R., Miller, J. B., Montzka, S., Sherwood, T., Saripalli, S., Sweeney, C., and Tans, P. P.: Assessment of fossil fuel carbon dioxide and other anthropogenic trace gas emissions from airborne measurements over Sacramento, California in spring 2009, Atmos. Chem. Phys., 11, 705-721, 2011.

U.S. EPA: National air quality and emissions trends report-2003 special studies edition. EPA/454/R-03/005. Research Triangle Park, NC, 2003.

US Department of Transportation: Highway Functional Classification: Concepts, Criteria and Procedures, Federal Highway Administration, Publication Number: FHWA-PL-13-026, 70 pp., 2013.

US Department of Transportation - Federal Highway Administration: FHWA Vehicle Types, https://www.fhwa.dot.gov/policy/ohpi/vehclass.htm, 2011, accessed online 2 April 2014.

US-EPA: National Emission Inventory NEI 2008, version 3 (released March 1, 2013), http://www.epa.gov/ttnchie1/net/2008inventory.html, accessed online April 20, 2014.

Vogel, F. R., Hammer, S., Steinhof, A., Kromer, B. And Levin, I.: Implication of weekly and diurnal ^{14}C calibration on hourly estimates of CO-based fossil fuel CO_2 at a moderately polluted site in southwestern Germany. Tellus B, 62: 512-520, 2010.

Wang, Y., Munger, J. W., Xu, S., McElroy, M. B., Hao, J., Nielsen, C. P., and Ma, H.: CO_2 and its correlation with CO at a rural site near Beijing: implications for combustion efficiency in China, Atmos. Chem. Phys., 10, 8881-8897, 2010.

Wang, R., Tao, S., Ciais, P., Shen, H. Z., Huang, Y., Chen, H., Shen, G. F., Wang, B., Li, W., Zhang, Y. Y., Lu, Y., Zhu, D., Chen, Y. C., Liu, X. P., Wang, W. T., Wang, X. L., Liu, W. X., Li, B. G., and Piao, S. L.: High-resolution mapping of combustion processes and implications for CO_2 emissions, Atmos. Chem. Phys., 13, 5189-5203, 2013.

Winderlich, J., Chen, H., Gerbig, C., Seifert, T., Kolle, O., Lavrič, J. V., Kaiser, C., Höfer, A., and Heimann, M.: Continuous low-maintenance CO2/CH4/H2O measurements at the Zotino Tall Tower Observatory (ZOTTO) in Central Siberia, Atmos. Meas. Tech., 3, 1113-1128, doi:10.5194/amt-3-1113-2010, 2010.

WMO: Guidelines for the measurement of atmospheric carbon monoxide, WMO TD No. 1551, GAW 192, available at: http://www.wmo.int/pages/prog/arep/gaw/gaw-reports.html (accessed online 28 October 2013), World Meteorological Organization, Geneva, Switzerland, 49 pp., 2010.

Wofsy, S.C.: Interactions of CH_4 and CO in the earth's atmosphere, Annu. Rev. Earth Pl. Sc., 4, 441-469, 1976.

Zhao, C., and Tans, P.: Estimating uncertainty of the WMO Mole Fraction Scale for carbon dioxide in air, J. Geophys. Res. 111, D08S09, doi: 10.1029/2005JD006003, 2006.